Elastic p-^{12}C scattering calculations using a cluster effective field theory

Eun Jin In,[1,2,3] Tae-Sun Park,[2,*] Young-Ho Song,[4] and Seung-Woo Hong[4,5]

[1]*Department of Energy Science, Sungkyunkwan University, Suwon 16419, Republic of Korea*
[2]*Center for Exotic Nuclei Studies, Institute for Basic Science, Daejeon 34126, Republic of Korea*
[3]*Nuclear and Chemical Sciences Division, Lawrence Livermore National Laboratory, Livermore, California 94551, USA*
[4]*Institute for Rare Isotope Science, Institute for Basic Science, Daejeon 34000, Republic of Korea*
[5]*Department of Physics, Sungkyunkwan University, Suwon 16419, Republic of Korea*

(Received 3 January 2024; revised 23 March 2024; accepted 30 April 2024; published 29 May 2024)

The elastic p-^{12}C scattering at low energies is studied by using a cluster effective field theory (EFT), where the low-lying resonance states ($s_{1/2}$, $p_{3/2}$, $d_{5/2}$) of ^{13}N are treated as pertinent degrees of freedom. The low-energy constants of the Lagrangian are expressed in terms of the Coulomb-modified effective range parameters, which are determined to reproduce the experimental data for the differential cross sections. The resulting theoretical predictions agree very well with the experimental data. The resulting theory is shown to give us almost identical phase shifts as obtained from the R-matrix approach and predict the experimental analyzing power data. The role of the ground state of ^{13}N below the threshold and the next-to-leading order in the EFT power counting are also discussed.

DOI: 10.1103/PhysRevC.109.054622

I. INTRODUCTION

The cluster effective field theory (EFT) [1,2] provides a powerful framework to describe low-energy nuclear dynamics, and recent developments make it an alternative approach to the R-matrix theory [3–6], which is widely used for the description of nuclear reactions. By exploiting the scale separation of the system, the cluster EFT provides a systematic expansion scheme of the theories, and thus allows improved calculations with well-defined error estimates. The cluster EFT has been used for the analysis of diverse nuclear systems, including the one-neutron halo nucleus ^{19}C [7], one-proton halo nuclei ^{17}F and ^{8}B [8,9]. It has also been applied to nonhalo systems with the existence of scale separation such as the resonant α-α scattering [10], ^{12}C-α scattering [11,12], and low energy radiative capture reactions, for example, ^{3}He$(\alpha,\gamma)^{7}$Li [13].

In the present work, we analyze the differential cross section for the low-energy elastic p-^{12}C scattering in the cluster EFT. The availability of accurate experimental data makes the elastic scattering of p-^{12}C a good testing ground for the cluster EFT and the R-matrix theory [6]. As we shall discuss shortly, the system has rather a big expansion parameter, which makes the convergence of the cluster EFT nontrivial. Another intriguing feature of the system is the existence of a subthreshold, i.e., the ground state of ^{13}N lies 1.9 MeV below the threshold. By performing a detailed study with and without the state, we will address the relevance of the subthreshold in the elastic scattering. As a test of our theory, the analyzing powers A_y are calculated by using the low-energy constants fitted to the elastic scattering data, and the resulting theoretical A_y is compared with the experimental data.

A study of the elastic scattering of p-^{12}C is also important as the first step towards the calculation of the radiative proton capture of ^{12}C, ^{12}C$(p,\gamma)^{13}$N, which plays an important role in the CNO cycle [14]. ^{12}C$(p,\gamma)^{13}$N$(\beta^{+})^{13}$C increases the ^{13}C abundance and thus through the ^{13}C$(\alpha,n)^{16}$O reaction would increase a neutron source in the asymptotic giant branch (AGB) stars [15]. Direct measurement of the reaction cross section at astrophysical energies is difficult due to the Coulomb barrier, and employing a theoretical model is needed to extrapolate the cross section at astrophysical energies. The reaction has been studied in diverse theoretical approaches, which include potential models like potential cluster model (PCM) [16], single-particle model [17], distorted wave Born approximation (DWBA) [18], and the phenomenological R-matrix theory [19]. Thus, in this work, we determine the low energy constants for the elastic scattering of p-^{12}C which are necessary for the future study of the radiative capture reaction.

This paper is organized as follows. In Sec. II, the cluster EFT formalisms for s-, p-, and d-wave interactions of elastic p-^{12}C scattering and renormalization conditions are given. In Sec. III, we present the renormalization procedure, the resulting phase shifts, and the analyzing powers, with discussions on the power counting and the comparison with the R-matrix results. In Sec. IV, we make conclusive remarks.

II. CLUSTER EFT FOR s-, p-, AND d-WAVE INTERACTIONS

Most of the formalism which is necessary for the description of elastic p-^{12}C scattering in the framework of cluster EFT can be found in Refs. [1,20]. In this section, we briefly

*tspark@ibs.re.kr

 ©2024 American Physical Society

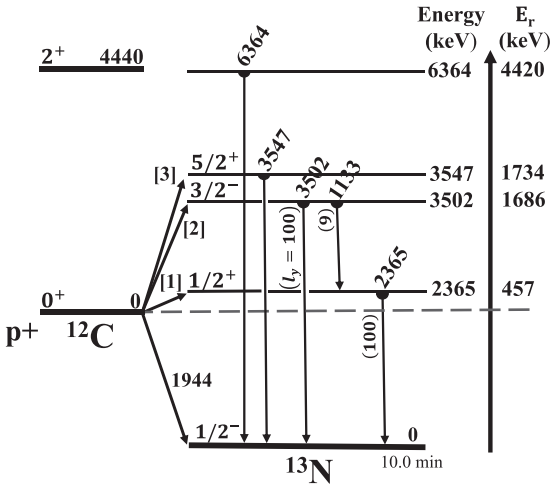

FIG. 1. Level scheme of ^{13}N (not to scale).

provide necessary expressions to facilitate presentation and discussion.

A. Scale separation and Lagrangian

Figure 1 depicts the level scheme of the compound nucleus ^{13}N. The three low-lying resonance states with $J^\pi = 1/2^+$, $3/2^-$, and $5/2^+$ of ^{13}N are taken as pertinent degrees of freedom of the theory. Their respective excitation energies are $E_r = 0.457$, 1.686, and 1.734 MeV, with corresponding momenta of $\sqrt{2m_{\rm R}E_r} = 28$, 54, 55 MeV, where $m_{\rm R}$ is the reduced mass of the p-^{12}C system. These momenta are characterized by the scale denoted as k_{lo}, which is regarded as small compared with the high momentum scale k_{hi}. The natural choice for k_{hi} is the momentum corresponding to the core excitation $\sqrt{2m_{\rm R}E^*} \sim 90$ MeV, where $E^* = 4.44$ MeV is the first excitation energy of ^{12}C. The EFT is then expanded with increasing power of the ratio $k_{lo}/k_{hi} = (0.3$–$0.6)$. The scale associated with the Coulomb interaction, $k_{\rm C} = Z_{\rm C}\alpha_{EM}m_{\rm R} \sim 38$ MeV, is numerically comparable to k_{lo}, where $Z_C = 6$ and $\alpha_{EM} \simeq 1/137.036$ is the fine structure constant. The ground state of ^{13}N with $J^\pi = 1/2^-$ is a subthreshold state located below the threshold, $E_r = -1.944$ MeV, and its role will be discussed later.

The effective Lagrangian for the system can be written as [21–23]

$$\begin{aligned}\mathcal{L} &= \psi_p^\dagger\left(iD_t + \frac{\vec{D}^2}{2m_p}\right)\psi_p + \psi_c^\dagger\left(iD_t + \frac{\vec{D}^2}{2m_c}\right)\psi_c \\ &+ \sum_x d_x^\dagger\left[\Delta_x + \sum_{n=1}^{N_x}\nu_{n,x}\left(iD_t + \frac{\vec{D}^2}{2m_{\rm tot}}\right)^n\right]d_x \\ &- \sum_x g_x[\,d_x^\dagger[\psi_p\, i\overleftrightarrow{\nabla}\,\psi_c\,]_x + \text{h.c.}] + \cdots, \end{aligned} \tag{1}$$

where ψ_p, ψ_c, and d_x are the proton, ^{12}C and the dicluster field, respectively, with the subscript d_x denoting the total angular momentum and parity of the dicluster, $x = J^\pi$. Their masses are denoted as m_p, m_c, and $m_{\rm tot} = m_p + m_c$, respectively, and the covariant derivatives are defined as

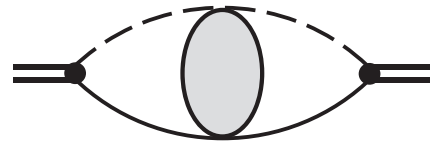

FIG. 2. Self-energy diagram of a dicluster. The solid line denotes the core (^{12}C) and the dashed line represents the proton field. The shaded bubble denotes the Coulomb Green's function.

$D_\mu = \partial_\mu + ie\hat{Q}A_\mu$, where $\hat{Q}$ is the charge operator. The parameters Δ_x and g_x represent the residual masses and coupling constants of field d_x, respectively. The index n is 1 for s and p waves, and runs up to 2 for the d wave. $\nu_{1,x}$ in the kinetic term of the dicluster field is chosen as ± 1 to denote the sign related to the effective range [1], while the $\nu_{2,x}$ in the second-order kinetic term for the d wave is needed for renormalization. At LO, we have therefore two low-energy constants (LECs) for s and p waves, and three low-energy constants for the d wave. As we shall show shortly, these LECs are to be related to the effective range parameters.

The projection of the operator $\psi_p\, i\nabla\psi_c = \psi_p(m_c i\vec{\nabla} - m_p i\vec{\nabla})\psi_c/(m_p + m_c)$ to the $x = 1/2^+,\ 3/2^-,\ 1/2^-$, and $5/2^+$ states are given as [24]

$$\begin{aligned}\left[\psi_p i\overleftrightarrow{\nabla}\psi_c\right]^m_{\frac{1}{2}^+} &= \sum_{m_s} C^{\frac{1}{2}m}_{00,\frac{1}{2}m_s}\,\psi_p\psi_c, \\ \left[\psi_p i\overleftrightarrow{\nabla}\psi_c\right]^m_{\frac{3}{2}^-\left(\frac{1}{2}^-\right)} &= \sum_{\alpha,m_s} C^{\frac{3}{2}m\left(\frac{1}{2}m\right)}_{1\alpha,\frac{1}{2}m_s}\,\psi_p i\overleftrightarrow{\nabla}_\alpha\psi_c, \\ \left[\psi_p i\overleftrightarrow{\nabla}\psi_c\right]^m_{\frac{5}{2}^+} &= \sum_{\alpha,\beta,m_l,m_s} C^{\frac{5}{2}m}_{2m_l,\frac{1}{2}m_s}C^{2m_l}_{1\alpha,1\beta}\psi_p \\ &\quad\times\frac{1}{2}\left(i\overleftrightarrow{\nabla}_\alpha i\overleftrightarrow{\nabla}_\beta + i\overleftrightarrow{\nabla}_\beta i\overleftrightarrow{\nabla}_\alpha\right)\psi_c, \end{aligned} \tag{2}$$

where m_s is the spin projection of the proton and $C^{Jm}_{j_1m_1,j_2m_2}$ is a short notation for the Clebsch-Gordan coefficients $\langle j_1m_1,\, j_2m_2|(j_1j_2)jm\rangle$. Here and hereafter, we use the Greek letters to denote spherical components that run from -1 to 1. The conversion to Cartesian coordinates for convenience in the calculation of the d wave can be found in Ref. [22].

B. The irreducible self-energy and renormalization conditions

The full dicluster propagator of the dicluster d_x reads

$$iD_x(E) = \frac{i}{\Delta_x + \sum_{n=1}^{N_x}\nu_{n,x}(E+i\epsilon)^n - \Sigma_x(E)}, \tag{3}$$

where $\Sigma_x(E)$ is the irreducible self-energy shown in Fig. 2. The Coulomb interaction plays a crucial role at low energy, and is taken into account by the Coulomb Green's function. Because each dicluster of x in our consideration has a different orbital angular momentum l, we will use l and x interchangeably hereafter.

The elastic scattering amplitude T_l for s, p, and d waves are depicted in Fig. 3, and can be evaluated as [12]

$$T_l = g_l^2 D_l(E)e^{2i\sigma_l}k^{2l}\hat{C}_l^2(\eta), \tag{4}$$

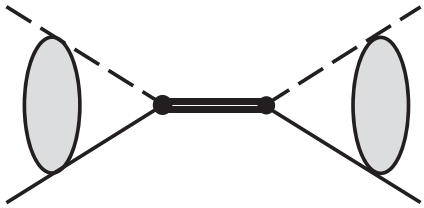

FIG. 3. Scattering amplitude for elastic p-^{12}C scattering. The notations are the same as in Fig. 2.

where $\sigma_l = \arg\Gamma(l+1+i\eta)$, and

$$\hat{C}_l(\eta) = |\Gamma(l+1+i\eta)|e^{-\frac{1}{2}\pi\eta}/\Gamma(l+1), \tag{5}$$

which is the Gamow-Sommerfeld factor $C_l(\eta)$ [8,26] but normalized to unity when η goes to zero.

The scattering amplitude in Eq. (4) can be matched with the effective range function as [10]

$$T_l(E) = -\frac{2\pi}{m_R}\frac{k^{2l}e^{2i\sigma_l}\hat{C}_l^2(\eta)}{f_l(k) - 2k_C h_l(\eta)}. \tag{6}$$

Here, $f_l(k)$ is the Coulomb-modified effective range function (ERF) [27–29] defined as

$$\begin{aligned} f_l(k) &\equiv k^{2l+1}\hat{C}_l(\eta)^2(\cot\delta_l(k) - i) + 2k_C h_l(\eta) \\ &= -\frac{1}{a_l} + \frac{1}{2}r_l k^2 - \frac{1}{4}P_l k^4 + \cdots, \end{aligned} \tag{7}$$

where δ_l is the phase shifts relative to the regular Coulomb function for angular momentum l, a_l, r_l, and P_l are the effective range parameters (scattering length, effective range, and shape parameter), and the function $h_l(\eta)$ is defined as [29,30]

$$h_l(\eta) = k^{2l}\frac{\hat{C}_l(\eta)^2}{\hat{C}_0(\eta)^2}\left(\psi(i\eta) + \frac{1}{2i\eta} - \log(i\eta)\right), \tag{8}$$

where $\psi(z) = \Gamma'(z)/\Gamma(z)$ is the logarithmic derivative of the Γ function. Comparison of Eq. (6) with Eq. (4) enables us to renormalize the LECs in terms of the effective range parameters.

1. S-wave interaction

The irreducible self-energy of s-wave dicluster can be expressed as

$$\begin{aligned} \Sigma_0(E) &= g_0^2\int\frac{d^3\boldsymbol{k}d^3\boldsymbol{k}'}{(2\pi)^6}\langle\boldsymbol{k}|G_C(E)|\boldsymbol{k}'\rangle \\ &= g_0^2\int\frac{d^3\boldsymbol{p}}{(2\pi)^3}\frac{\psi_{\boldsymbol{p}}(0)\psi_{\boldsymbol{p}}^*(0)}{E - p^2/2m_R + i\epsilon}, \end{aligned} \tag{9}$$

where $G_C(E)$ is the Coulomb Green's function [29],

$$\langle\mathbf{r}|G_C(E)|\mathbf{r}'\rangle = \int\frac{d^3\boldsymbol{p}}{(2\pi)^3}\frac{\psi_{\boldsymbol{p}}(\mathbf{r})\psi_{\boldsymbol{p}}^*(\mathbf{r}')}{E - \frac{p^2}{2m_R} + i\epsilon}, \tag{10}$$

and $\psi_{\boldsymbol{p}}(\mathbf{r})$ is the Coulomb wave function

$$\psi_{\boldsymbol{p}}(\mathbf{r}) = \sum_{l=0}^{\infty}(2l+1)i^l e^{i\sigma_l}\frac{F_l(\eta, pr)}{pr}P_l(\hat{p}\cdot\hat{r}) \tag{11}$$

with $\eta = k_C/p$ and F_l being the regular Coulomb functions [31].

The integral in Eq. (9) can be evaluated by using the power divergence subtraction (PDS) method [29,32,33],

$$\Sigma_0(E) = -g_0^2\frac{k_C m_R}{\pi}h_0(\eta) + \Sigma_0^{\rm div}, \tag{12}$$

and the divergent part $\Sigma_0^{\rm div}$ is energy-independent, whose explicit form can be found in Refs. [32,33].

The s-wave ERF with $l = 0$ is then given as

$$f_0(k) = -\frac{2\pi}{g_0^2 m_R}\left(\Delta_0 + \Sigma_0^{\rm div}\right) - \frac{\pi\nu_0}{g_0^2 m_R^2}k^2. \tag{13}$$

Comparison of Eq. (13) with Eq. (6) gives us the renormalization conditions

$$\begin{aligned} \frac{1}{a_0} &= \frac{2\pi}{g_0^2 m_R}\left(\Delta_0 + \Sigma^{\rm div}\right), \\ r_0 &= -\frac{2\pi\nu_0}{g_0^2 m_R^2}. \end{aligned} \tag{14}$$

2. P-wave interaction

By using a similar procedure as for the s wave, the irreducible self-energy of p-wave dicluster can be derived as [1]

$$\begin{aligned} \Sigma_1(E) &= \frac{1}{3}g_1^2\int\frac{d^3\boldsymbol{p}}{(2\pi)^3}\frac{p^2\hat{C}_1(\eta_p)^2}{E - \frac{p^2}{2m_R} + i\epsilon} \\ &= g_1^2\frac{m_R}{3\pi^2}\Big[-L_3 - \left(k^2 + k_C^2\right)L_1 \\ &\quad + k^2\left(k^2 + k_C^2\right)\int dp\frac{\hat{C}_0(\eta)^2}{k^2 - p^2 + i\epsilon}\Big] \\ &= \frac{g_1^2 m_R}{6\pi}\left[-\frac{2}{\pi}L_3 - \frac{2}{\pi}\left(k^2 + k_C^2\right)L_1 - 2k_C h_1(\eta)\right], \end{aligned} \tag{15}$$

where

$$L_n = \int dp\,\hat{C}_0(\eta_p)^2 p^{n-1}. \tag{16}$$

It is then a simple task to show that the resulting p-wave ERF reads $f_1(k) = -\frac{1}{a_1} + \frac{1}{2}r_1 k^2$ with

$$\begin{aligned} \frac{1}{a_1} &= -\frac{6\pi}{m_R}\left(\frac{\Delta_1}{g_1^2} - \frac{m_R}{3\pi^2}L_3 - \frac{m_R}{3\pi^2}k_C^2 L_1\right), \\ r_1 &= \frac{6\pi\nu_1}{g_1^2 m_R^2} - \frac{4}{\pi}L_1. \end{aligned} \tag{17}$$

3. D-wave interaction

By adopting the trick of using Cartesian representation of the d-wave vertex function [23,34], the irreducible self-energy of the d-wave dicluster can be evaluated as

$$\Sigma_2(E) = g_2^2 \frac{2}{15} \int \frac{d^3p}{(2\pi)^3} \frac{p^4 \hat{C}_2(\eta_p)^2}{E - \frac{p^2}{2m_R} + i\epsilon}$$
$$= \frac{g_2^2 m_R}{15\pi} \left[\left(-\frac{8}{\pi} L_5 - \frac{10}{\pi} k_C^2 L_3 - \frac{2}{\pi} k_C^4 L_1 \right) + \left(-\frac{8}{\pi} L_3 - \frac{10}{\pi} k_C^2 L_1 \right) k^2 - \frac{8}{\pi} L_1 k^4 - 2k_C h_2(\eta) \right]. \quad (18)$$

The corresponding d-wave ERF is then given as $f_2(k) = -\frac{1}{a_2} + \frac{1}{2} r_2 k^2 - \frac{1}{4} P_2 k^4$ with

$$\frac{1}{a_2} = \frac{15\pi}{g_2^2 m_R} \Delta_2 + \frac{8}{\pi} L_5 + \frac{10}{\pi} k_C^2 L_3 + \frac{2}{\pi} k_C^4 L_1,$$
$$r_2 = -\frac{15\pi \nu_{1,2}}{g_2^2 m_R^2} - \frac{16}{\pi} L_3 - \frac{20}{\pi} k_C^2 L_1,$$
$$P_2 = \frac{15\pi \nu_{2,2}}{m_R^3 g_2^2} + \frac{32}{\pi} L_1. \quad (19)$$

III. NUMERICAL RESULTS AND DISCUSSION

A. Fitting to experimental data

In the previous section, we have shown that the cluster EFT description with the LECs is equivalent to the Coulomb-modified ERF with a finite number of effective range parameters (ERPs), and the remaining task is to determine the values of the parameters. Although one could use the existing R-matrix phase shift analysis, we attempted to determine the LECs directly from the experimental data to show the effectiveness of EFT approach. We find that the fitting for the ERPs is complicated due to the strong correlations between the ERPs of the p and d waves, which is caused mainly by the fact that their pole positions are very close to each other. This problem can be avoided by rewriting the effective range function as a series around the pole position,

$$f_l(k) = -\frac{1}{a_l} + \frac{1}{2} r_l k^2 - \frac{1}{4} P_l k^4 + Q_l k^6 + \cdots$$
$$= \frac{1}{2} r_l' (k^2 - k_r^2) - \frac{1}{4} P_l' (k^2 - k_r^2)^2 + Q_l' (k^2 - k_r^2)^3 + \cdots, \quad (20)$$

where $k_r^2 \equiv 2m_R E_r'$, and $(E_r', r_l', P_l', Q_l', \ldots)$ are another representation of the ERPs $(a_l, r_l, P_l, Q_l, \ldots)$. It is to be noted that the values of E_r' are shifted from the actual pole positions (E_r) due to the term $-2k_C h_l(\eta)$ in the denominator of the scattering amplitude, Eq. (6), but as we will show below, this reparametrization is sufficient to remove the aforementioned correlation.

The parameters $(E_r', r_l', P_l', Q_l', \ldots)$ are determined by minimizing χ_Λ^2 defined as

$$\chi_\Lambda^2 = \sum_i^N \frac{|y_{i,\text{th}} - y_{i,\text{exp}}|^2}{\Delta y_{i,\text{exp}}^2 + \Delta y_{i,\text{th}}^2}, \quad (21)$$

where $y_{i,\text{exp}}$ $(y_{i,\text{th}})$ is the experimental (theoretical) differential cross sections at a given angle, $\Delta y_{i,\text{exp}}$ are error bars of the data. Some of the data have very small $\Delta y_{i,\text{exp}}$, and the usual χ square is dominated by them. As a regulator that takes into account the theoretical uncertainty, we introduce

$$\Delta y_{i,\text{th}} \equiv y_{i,\text{exp}} \times \frac{k_i}{\Lambda}, \quad (22)$$

where Λ is a parameter. While constructed in an ad hoc manner, this form is motivated by the fact that the EFT description is less accurate at high momentum. $\Delta y_{i,\text{th}}$ should not be bigger than the uncertainty of the theory, and thus we choose $\Lambda = 1$ GeV. The resulting parameters are found to be stable and insensitive to the values of Λ, while the value of χ_Λ^2 increases with Λ.

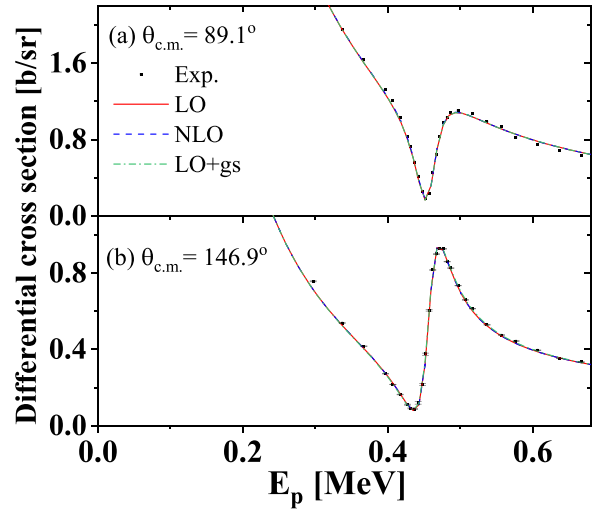

FIG. 4. The differential cross sections for elastic p-^{12}C scattering as a function of the proton energy $E_p < 0.7$ MeV at two angles (a) 89.1° and (b) 146.9°. The red, blue, and green solid lines represent the EFT results at LO, NLO, and LO+g.s. The black circles represent the experimental data [35].

So far, we have considered only the leading order (LO) terms, and the resulting theory turns out to be identical to the Coulomb-modified effective range expansion with the parameters (E_r', r_l') for s and p waves and (E_r', r_l', P_l') for the d wave. While we do not describe explicitly here, going to the next order (or NLO) with including one higher-order terms in the Lagrangian is also identical to the effective range expansion with one more term, that is, (E_r', r_l', P_l') for s and p waves and (E_r', r_l', P_l', Q_l') for the d wave, which we denote as NLO. We also perform the leading order calculation where the $J^\pi = \frac{1}{2}^-$ ground state of ^{13}N is taken as a pertinent degree of freedom, which we denote as LO+g.s. We thus have three sets of parameters, LO, NLO, and LO+g.s.

The parameters of each set are then fitted to reproduce the differential cross section data at three different angles, 89.1, 118.7, and 146.9 degrees [35]. Figures 4 and 5 show the resulting differential cross sections in the region $E_p \leqslant 0.7$ MeV and $E_p = (0.7–2)$ MeV, where E_p is the incident proton energy. The calculated cross sections agree very well with the data, which can also be seen in the obtained χ_Λ^2/datum = 1.20 for LO, and 1.03 for NLO.

The values of the fitted ERE parameters for the expansion around the origin are summarized in Table I. In the NLO

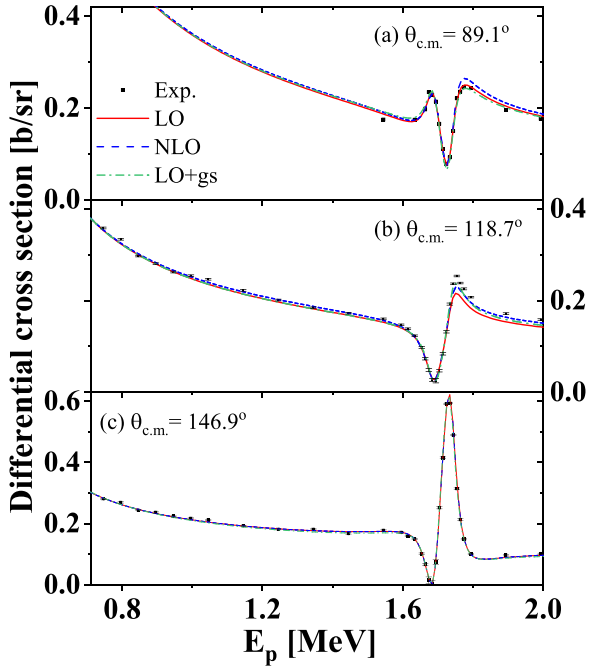

FIG. 5. The differential cross section for elastic p- ^{12}C scattering as a function of the proton energy $E_p = (0.7–2)$ MeV at three angles (a) 89.1°, (b) 118.7°, and (c) 146.9°. The notation is the same as in Fig. 4.

case, compared to LO, the added parameters, the P_1' for the $p_{3/2}$ wave and the P_2' and Q_2' for the $d_{5/2}$ wave, have large uncertainties that are much bigger than the central values. This might be due to a strong correlation between the parameters of $p_{3/2}$ and $d_{5/2}$ waves, which is not surprising since the pole positions at 1.686 and 1.734 MeV, respectively, are very close to each other.

Considering the role of the ground state on the differential cross sections, our results show that including the ground state provides a more accurate description of differential cross

TABLE I. The ERE parameters for the expansion around the pole positions. $Q_l' = (-27 \pm 99)$ fm for $d_{5/2}$ at NLO, and 0 for other cases.

	E_r' (MeV)	r_l' (fm^{1-2l})	P_l' (fm^{3-2l})
(a) LO			$\chi^2_\Lambda/N = 1.20$
$s_{1/2}$	-0.094 ± 0.001	1.521 ± 0.004	
$p_{3/2}$	1.743 ± 0.004	-1.828 ± 0.041	
$d_{5/2}$	1.764 ± 0.009	-0.194 ± 0.018	4.9 ± 2.7
(b)NLO			$\chi^2_\Lambda/N = 1.03$
$s_{1/2}$	-0.109 ± 0.002	1.447 ± 0.006	-2.55 ± 0.11
$p_{3/2}$	1.734 ± 0.019	-2.052 ± 0.419	30 ± 57
$d_{5/2}$	1.765 ± 0.016	-0.192 ± 0.041	5.39 ± 9.75
(c) LO+gs			$\chi^2_\Lambda/N = 1.01$
$s_{1/2}$	-0.094 ± 0.001	1.520 ± 0.004	
$p_{3/2}$	1.736 ± 0.004	-1.908 ± 0.040	
$d_{5/2}$	1.768 ± 0.011	-0.178 ± 0.021	2.1 ± 2.9
$p_{1/2}$	-1.02 ± 12.97	-0.20 ± 0.98	

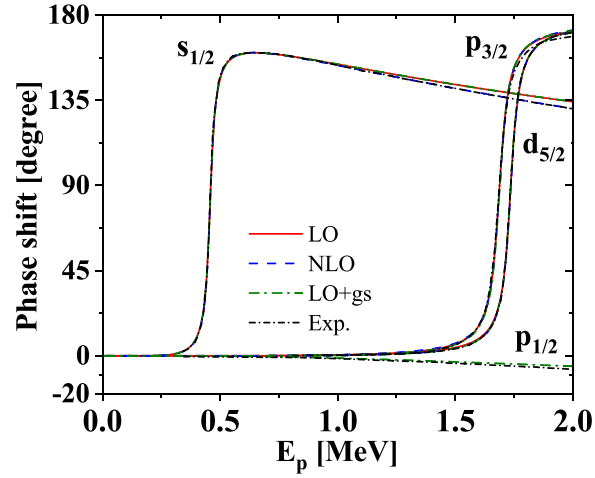

FIG. 6. The phase shifts. The red, green, and blue lines are for LO, NLO, and LO+g.s., respectively. The black short-dashed lines are the results by using the R matrix taken from Ref. [19].

section in the higher energy region, particularly around 1.7 MeV. Our result is in line with the finding obtained from the R-matrix study given in Ref. [19]. Figure 6 shows that the ground state gives us a small and slowly varying repulsive contribution. As can be seen in Table I, the pole position parameter for this channel suffers from a very big uncertainty, $E_r' = (-1 \pm 13)$ MeV, which is not surprising recalling that the ground state lies about 1.9 MeV below the threshold.

Let us now discuss the power counting of the obtained ERE parameters. For the s-wave cases, the ERE parameters listed in Table II suggest to count $a_0 \sim \frac{\Lambda^2}{Q^3}$, $r_0 \sim 1/\Lambda$, and $P_0 \sim 1/\Lambda^3$. That is, while r_0 (and P_0 in NLO) is in natural size, the s-wave scattering length a_0 is unnaturally large. As can be seen in Table I, this results in a very small E_0', $E_0' \simeq \frac{Q^3}{\Lambda^2}$, which could be possible due to a strong cancellation between the effective

TABLE II. The unprimed ERE parameters (a_l, r_l, P_l, Q_l). $Q_l' = (-27 \pm 99)$ fm for $d_{5/2}$ at NLO, and 0 for the other cases.

	a_l (fm^{1+2l})	r_l (fm^{1-2l})	P_l (fm^{3-2l})
(a) LO			$\chi^2_\Lambda/N = 1.20$
$s_{1/2}$	-315 ± 3	1.521 ± 0.004	
$p_{3/2}$	-14.1 ± 0.3	-1.83 ± 0.04	
$d_{5/2}$	-26 ± 11	0.19 ± 0.21	4.9 ± 2.7
(b) NLO			$\chi^2_\Lambda/N = 1.03$
$s_{1/2}$	-290 ± 6	1.46 ± 0.01	-2.55 ± 0.11
$p_{3/2}$	-4 ± 5	0 ± 4	30 ± 57
$d_{5/2}$	-19 ± 27	0 ± 4	-20 ± 94
(c) LO+gs			$\chi^2_\Lambda/N = 1.01$
$s_{1/2}$	-315 ± 4	1.520 ± 0.004	
$p_{3/2}$	-13.6 ± 0.3	-1.91 ± 0.04	
$d_{5/2}$	-49 ± 43	0.00 ± 0.23	2.1 ± 2.9
$p_{1/2}$	0.2 ± 3.0	-0.2 ± 1.0	
(d) 1992NPA Baumann			
$s_{1/2}$	104 ± 8	2.5 ± 0.1	15.9 ± 0.7
$p_{1/2}$	-464 ± 50	-0.10 ± 0.10	4.1 ± 1.8

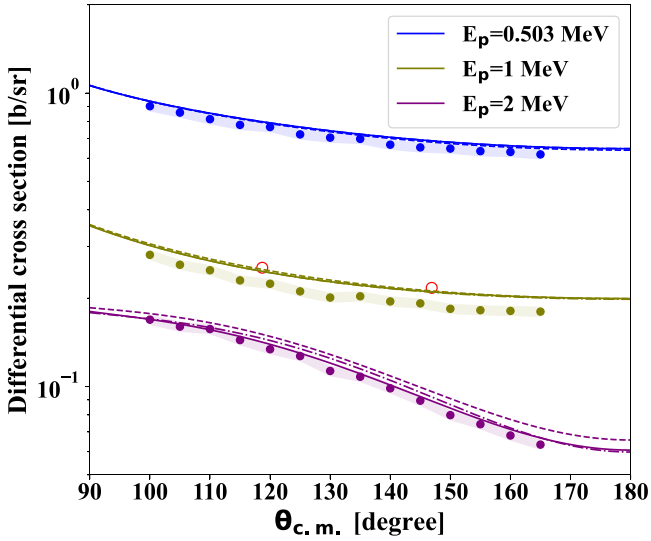

FIG. 7. Differential cross sections as a function of angles in the c.m. system at three representative proton energies, $E_p = 0.503$, 1, and 2 MeV are plotted by the filled circles. The results from our EFT at these energies are represented by the blue, olive, and purple lines, respectively. The solid, dashed, and dashed-dotted lines correspond to the EFT results at LO, NLO, and LO+g.s., respectively. The experimental data taken from Ref. [38] are represented by the filled circles. For a discussion (see text), we also marked the experimental data measured at $E_p = 0.996$ MeV given in Ref. [35] by the empty red circles.

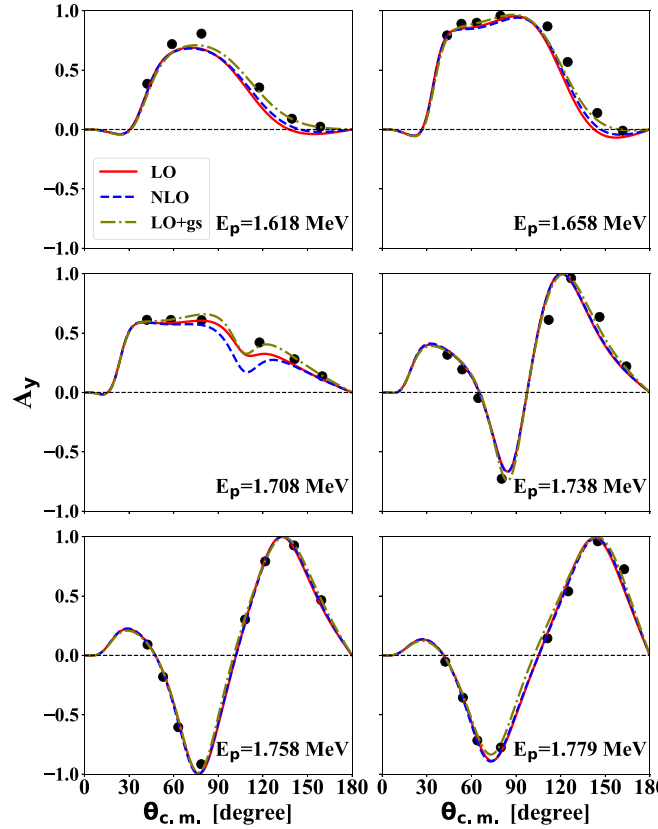

FIG. 8. The analyzing power A_y for the elastic p-^{12}C scattering for energies at 1.618, 1.658, 1.708, 1.738, 1.758, and 1.779 MeV. The red solid, blue dashed, and olive dashed-dotted lines correspond to the EFT results at LO, NLO, and LO+g.s., respectively. The experimental data taken from Ref. [37] are represented by the filled circles.

range term and the Coulomb term, $\frac{1}{2}r_0k^2 - 2k_Ch_0(\eta) \sim \frac{Q^3}{\Lambda^2}$ near the resonance energy. This is similar to the observation for α-^{3}He scattering in Ref. [36]. On the other hand, $p_{3/2}$ channel results correspond to $a_1 \sim \frac{1}{\Lambda Q^2}$ and $r_1 \sim \Lambda$. Note that for the p wave, the Coulomb contribution is very small: $\sim 2k_Ch_1(\eta) \sim \frac{Q^4}{\Lambda}$. Unfortunately, large uncertainties in the fitted parameters in $d_{5/2}$ and $p_{1/2}$ channels make it difficult to say any concrete discussion on power counting for those channels.

The phase shifts are plotted and compared with the R-matrix analysis in Fig. 6. As can be seen in Fig. 6, our results are very close to those obtained by R-matrix calculations [19]. However, the obtained scattering length and effective range parameter values in $s_{1/2}$ channel show large discrepancies from those in Ref. [37]. Considering a good description of the cross section in our calculation and the fact that Ref. [37] only used data in the range $1 < E < 2$ MeV, those ERE parameters might need to be updated.

As a test of our theory, we have calculated differential cross sections and compared them with the experimental data [38] at three representative proton energies, i.e., at $E_p = 0.503$, 1, and 2 MeV. In Fig. 7, the experimental data [38] are plotted by the filled circles. They are known to have uncertainties up to $\pm 4\%$, which is indicated by the shaded regions in the figure. Our theoretical predictions are in good agreement with the data at $E_p = 0.503$ and 2 MeV, while a slight overprediction is observed at $E_p = 1$ MeV. However, this gap should be interpreted with caution, since our results are in excellent agreement with the experimental data given in Ref. [19] at almost the same energy ($E_p = 0.996$ MeV) measured at $\theta_{\text{c.m.}} = 118.7$ and 146.9 degrees, which are marked by the empty red circles in Fig. 7.

We also apply our theory to the analyzing power A_y (see Refs. [13,37] and the references therein for details),

$$A_y = \frac{\frac{d\sigma}{d\Omega}_{\uparrow} - \frac{d\sigma}{d\Omega}_{\downarrow}}{\frac{d\sigma}{d\Omega}_{\uparrow} + \frac{d\sigma}{d\Omega}_{\downarrow}}. \tag{23}$$

As can be seen in Fig. 8, a very good agreement is achieved with the experimental values [37]. We observe that the "LO+g.s." (dotted-dashed lines) again gives us better agreement than LO (red solid lines) and NLO (blue dashed lines). It is remarkable that the agreement in A_y is achieved without introducing any additional parameter nor any refit.

IV. CONCLUSIONS

The elastic p-^{12}C scattering at energies below $E_p \leqslant 2$ MeV is studied in terms of a cluster EFT, the pertinent degrees of freedom of which are the proton, the ground state of ^{12}C, and the three low-lying states ($s_{1/2}$, $p_{3/2}$, $d_{5/2}$) of ^{13}N. The resulting scattering amplitudes of the theory are found

to be consistent with the Coulomb-modified ERE, and the low-energy constants are represented by the ERE parameters. At the leading order, we have seven parameters, two for each of the s and p waves, and three for the d wave. The theory prediction turns out to be in a very good agreement with the experimental data, achieving χ^2_Λ/datum $= 1.20$ [see Eqs. (21), (22) for the definition of χ^2_Λ].

The fitting procedure for the ERE parameters can be substantially simplified by expanding the ERE around the pole positions and defining the ERE parameters accordingly, which strongly reduces correlations among the parameters. The effect of the higher-order terms has been studied by adding one higher-order term for each partial wave, which is denoted as NLO and scores χ^2_Λ/datum $= 1.03$. To estimate the role of the ground state of ^{13}N that lies below the threshold, we have also considered the cases where the ground state is promoted to an explicit degree of freedom. The resulting "LO+g.s." theory results in χ^2_Λ/datum $= 1.01$. These improvements of NLO and LO+g.s. are, however, accompanied by large uncertainties in the additionally introduced ERE parameters (see Table I). It shows that the experimental data considered in this work with $E_p \leqslant 2$ MeV are well described by the LO, and the contributions from the higher-order terms and the subthreshold ground state are not essential. The resulting phase shifts are in an excellent agreement with the R-matrix analysis [19].

The experimental values of the differential cross sections and the analyzing power A_y with respect to the angles could be well reproduced by our theory as shown in Figs. 7 and 8 without introducing any additional parameters or performing any further fitting of the parameters. Such a prediction of not only the differential cross sections but also the analyzing power with respect to the angles can be considered as an indirect validation of the theory.

The high momentum scale of a low-energy EFT is set by the lowest-energy state that is not taken explicitly: 2^+ state of ^{12}C with $E_x = 4.44$ MeV and $d_{5/2}$ state of ^{13}N with $E_x = 6.36$ MeV. This corresponds to rather a large expansion parameter $k_{lo}/k_{hi} = (0.3\text{–}0.6)$. The theory could be extended to include these states as pertinent degrees of freedom as well, which would give us a lower expansion parameter. However, such an extension by limiting ourselves to a low-energy region would give us only a marginal improvement. The main mechanism that makes our approach successful despite this rather large ratio might be traced to the relevance of the ERE at low energies. As discussed earlier, a natural extension of this work would be the radiative capture ^{12}C$(p, \gamma)^{13}$N reaction.

ACKNOWLEDGMENTS

This work was supported in part by the Korean government Ministry of Science and ICT (MSIT) through the National Research Foundation (2020R1A2C1102384) and in part by the Institute for Basic Science (IBS-R031-D1). The work of Y.-H.S. was supported by the National Research Foundation of Korea (NRF) funded by Ministry of Science and ICT(2013M7A1A1075764, RS-2022-00165168) and by the National Supercomputing Center with supercomputing resources including technical support (KSC-2021-CRE-0429, KSC-2023-CRE-0006). The work of E.J.I. was prepared in part by LLNL under Contract No. DE-AC52-07NA27344.

[1] C. Bertulani, H.-W. Hammer, and U. Van Kolck, Nucl. Phys. A **712**, 37 (2002).
[2] H. Hammer, C. Ji, and D. Phillips, J. Phys. G: Nucl. Part. Phys. **44**, 103002 (2017).
[3] E. P. Wigner and L. Eisenbud, Phys. Rev. **72**, 29 (1947).
[4] A. Lane and R. Thomas, Rev. Mod. Phys. **30**, 257 (1958).
[5] P. Descouvemont and D. Baye, Rep. Prog. Phys. **73**, 036301 (2010).
[6] T.-S. Park, Phys. Rev. C **104**, 064612 (2021).
[7] B. Acharya and D. R. Phillips, Nucl. Phys. A **913**, 103 (2013).
[8] E. Ryberg, C. Forssén, H.-W. Hammer, and L. Platter, Phys. Rev. C **89**, 014325 (2014).
[9] X. Zhang, K. M. Nollett, and D. Phillips, Phys. Lett. B **751**, 535 (2015).
[10] R. Higa, H.-W. Hammer, and U. Van Kolck, Nucl. Phys. A **809**, 171 (2008).
[11] S.-I. Ando, Eur. Phys. J. A **52**, 130 (2016).
[12] S.-I. Ando, Phys. Rev. C **97**, 014604 (2018).
[13] M. Poudel and D. R. Phillips, J. Phys. G: Nucl. Part. Phys. **49**, 045102 (2022).
[14] M. Agostini *et al.* (The BOREXINO Collaboration), Nature (London) **587**, 577 (2020).
[15] N. Mowlavi, A. Jorissen, and M. Arnould, Astron. Astrophys. **334**, 153 (1998).
[16] A. Kabir, B. Irgaziev, and J.-U. Nabi, Braz. J. Phys. **50**, 112 (2020).
[17] J. Huang, C. Bertulani, and V. Guimaraes, At. Data Nucl. Data Tables **96**, 824 (2010).
[18] Z. Li, J. Su, B. Guo, Z. Li, X. Bai, J. Liu, Y. Li, S. Yan, B. Wang, Y. Wang *et al.*, Sci. China: Phys. Mech. Astron. **53**, 658 (2010).
[19] R. E. Azuma, E. Uberseder, E. C. Simpson, C. R. Brune, H. Costantini, R. J. de Boer, J. Görres, M. Heil, P. J. LeBlanc, C. Ugalde, and M. Wiescher, Phys. Rev. C **81**, 045805 (2010).
[20] H.-W. Hammer, S. König, and U. van Kolck, Rev. Mod. Phys. **92**, 025004 (2020).
[21] E. Ryberg, C. Forssén, H.-W. Hammer, and L. Platter, Eur. Phys. J. A **50**, 170 (2014).
[22] P. Bedaque, H.-W. Hammer, and U. Van Kolck, Phys. Lett. B **569**, 159 (2003).
[23] J. Braun, W. Elkamhawy, R. Roth, and H. Hammer, J. Phys. G: Nucl. Part. Phys. **46**, 115101 (2019).
[24] M. Tanabashi, K. Hagiwara, K. Hikasa, K. Nakamura, Y. Sumino, F. Takahashi, J. Tanaka, K. Agashe, G. Aielli, C. Amsler *et al.* (Particle Data Group), Phys. Rev. D **98**, 030001 (2018).

[26] M. X. Abramowitz and I. A. Stegun, Handbook of Mathematical Functions (Harri Deutsch, Thun, Frankfurt/Main, 1984).
[27] R. O. Berger and L. Spruch, Phys. Rev. **138**, B1106 (1965).
[28] S. König, Effective quantum theories with short- and long-range forces, Ph.D. thesis, Universität Bonn, 2013.
[29] X. Kong and F. Ravndal, Nucl. Phys. A **665**, 137 (2000).
[30] J. D. Jackson and J. M. Blatt, Rev. Mod. Phys. **22**, 77 (1950).
[31] S. König, D. Lee, and H. Hammer, J. Phys. G: Nucl. Part. Phys. **40**, 045106 (2013).
[32] X. Kong and F. Ravndal, Phys. Lett. B **450**, 320 (1999).
[33] S.-i. Ando, J. W. Shin, C. H. Hyun, and S.-W. Hong, Phys. Rev. C **76**, 064001 (2007).
[34] L. S. Brown and G. M. Hale, Phys. Rev. C **89**, 014622 (2014).
[35] H. Meyer, G. Plattner, and I. Sick, Z. Phys. A: At. Nucl. **279**, 41 (1976).
[36] R. Higa, G. Rupak, and A. Vaghani, Eur. Phys. J. A **54**, 89 (2018).
[37] R. Baumann, G. Keil, N. Kniest, E. Pfaff, M. Preiss, M. Skill, and G. Clausnitzer, Nucl. Phys. A **542**, 53 (1992).
[38] S. Mazzoni, M. Chiari, L. Giuntini, P. Mandò, and N. Taccetti, Nucl. Instrum. Methods Phys. Res. B **136–138**, 86 (1998).